

Communication

High Performance Dual-Core D-Shaped PCF Refractive Index Sensor Coated with Gold Grating

Yu Ying ¹, You Xia ¹, Siyu Cheng ¹, Dan Shan ¹, Zhijun Gao ^{1,*}, Guangyuan Si ² and Xiaoxi Tian ²

¹ College of Electrical & Control Engineering, Shenyang Jianzhu University, Shenyang 110168, China

² Melbourne Centre for Nanofabrication, Victorian Node of the Australian National Fabrication Facility, Clayton, VIC 3168, Australia

* Correspondence: gzj@sjzu.edu.cn

Abstract: In this study, a dual-core D-shaped photonic crystal fiber (PCF) surface plasmon resonance sensor coated with gold grating is designed and analyzed using the finite-element method (FEM). The surface plasmon resonance (SPR) effect between the fiber core modes and surface plasmon polariton (Spp) modes is used to measure the analyte refractive index. The effects of the PCF structure parameters (polishing depths, large holes, and small holes) and grating parameters (grating heights, grating periods, and grating duty) are discussed, and a two-feature interrogation method that combines wavelength and intensity interrogations is introduced to enhance the resolution. The results show that the grating and dual-core play important roles in enhancing the sensor properties. The proposed sensor achieves an average wavelength sensitivity of 994.5 nm/RIU when the analyte refractive index increases from 1.33 to 1.37. Furthermore, a maximum amplitude sensitivity of 181.049 RIU⁻¹ is obtained. The two-feature interrogation is determined to have a resolution of 2.03×10^{-6} RIU, which is better than the wavelength and amplitude interrogations. The proposed sensor has a good sensing performance and is highly suitable for practical applications.

Keywords: dual-core; photonic crystal fiber; grating; finite element method



Citation: Ying, Y.; Xia, Y.; Cheng, S.; Shan, D.; Gao, Z.; Si, G.; Tian, X. High Performance Dual-Core D-Shaped PCF Refractive Index Sensor Coated with Gold Grating. *Photonics* **2023**, *10*, 473. <https://doi.org/linebreak/10.3390/photonics10040473>

Received: 16 March 2023

Revised: 13 April 2023

Accepted: 18 April 2023

Published: 20 April 2023



Copyright: © 2023 by the authors. Licensee MDPI, Basel, Switzerland. This article is an open access article distributed under the terms and conditions of the Creative Commons Attribution (CC BY) license (<https://creativecommons.org/licenses/by/4.0/>).

1. Introduction

Optical fiber-based surface plasmon resonance (SPR) has attracted considerable attention from researchers owing to its advantages of anti-electromagnetic interference, small-size, and real-time monitoring [1–3]. In recent years, optical fiber-based SPR sensor technology has been widely used in areas such as food quality detection, chemical analyte analysis, magnetic field detection, and environmental measurements [4–9]. In addition, SPR biosensors are already in the stage of large-scale application [10,11]. Compared with prism-based SPR sensors (Kretschmann configuration), optical fiber-based SPR structures exhibit a compact size, low cost, and high degree of integration, which can enable their application in narrow spaces, remote measurements, distributed measurements, and real-time detections [12–14]. With the development of photonic crystal fiber (PCF) sensors, it has been found that the fiber core can be designed to have a large mode field diameter, increasing the interaction volume between light and samples, and improving sensitivity. Consequently, someone proposed that SPR could be combined with PCF to achieve a better effect [15–17]. PCF has the advantages of a large mode area, flexible control, and high birefringence owing to its unique microstructure; hence, the SPR-PCF sensor can achieve improved sensing performance. SPR-PCF sensors can be realized by selectively filling liquid or coating metal inside an air hole. Chaudhary presented a PCF with two small air holes along the horizontal axis [18]. By investigating the filter characteristics, the proposed PCF showed single-polarization filtering in two communication bands of 1.63 and 1.378 μm . These features make it possible to realize a link between optical fiber sensing and communication. Guo presented an SPR-PCF refractive index sensor with a

nanoscale metal film coated on one side of cladding air holes [19]. The metal film could effectively eliminate interference between adjacent channels. The result shows that an average refractive index of 1931.03 nm/RIU (Refractive Index Unit) is obtained with a wide range of 1.35–1.46 by using the nanoscale metal film. Yang presented a symmetrical dual-layer SPR-PCF sensor with airholes arranged in a specific pattern and coated with a composite material [20]. The energy was divided into four channels coupled with surface plasmon polariton (Spp) modes, which enhanced the interaction between the plasmonic and fundamental modes, resulting in a maximum figure of merit (FOM) of 480 RIU⁻¹. It can be seen that the SPR-PCF sensor exhibits good performance when the air holes are filled with the composite material. However, in practical applications, this is a highly challenging and difficult task to accomplish.

To achieve better sensing performance, the D-shaped PCF is fabricated by side-polishing any region of the cladding side of the fiber, which improves the sensitivity of the fiber core mode to the external analyte refractive index. In recent studies, the optimization of the fiber core and metal film of a D-shaped PCF has been an important direction, such as some relevant studies that have been conducted to access the effectiveness of structural parameter optimization [21]. To optimize the fiber core, Sakib presented a highly sensitive dual-core D-shaped PCF sensor [22]. The pitch parameter and gold film thickness were optimized at 1.9 μm and 30 nm, respectively, and the maximum wavelength and amplitude sensitivities could reach 8000 nm/RIU and 700 RIU⁻¹, respectively. Jabin presented a dual-core D-shaped PCF with a splitting barrier between the two fiber cores [23]. The guide characteristics of the dual-core and single-core models were compared, and the results showed that the sensing performance of the dual-core model outperformed the single-core model. Singh presented an SPR D-shaped PCF sensor with a dual-core symmetrically polished surface [24]. Micro-openings were introduced, and four separate flat sensing channels were investigated; the results showed that the maximum refractive index resolution could reach up to 4.37×10^{-6} RIU. The introduction of a grating is an effective method for optimizing metal films. Lu presented a D-shaped PCF SPR sensor coated with gold grating [25]. Modulation of the resonance wavelength and enhancement of the refractive index sensitivity were investigated, the results showed that a resolution of 5.98×10^{-6} RIU could be obtained in the refractive index range of 1.36–1.38. Fang presented a highly sensitive D-shaped PCF sensor based on Ag-TiO₂ composite micro-gratings [26]. The response characteristic of the refractive index was studied using the finite element method (FEM), and a maximum FOM of 480 RIU⁻¹ could be obtained for optimal parameter optimization. The above research indicates that optimizing the fiber core or introducing grating can enhance the sensing performance of the D-shaped PCF, including sensitivity, resolution, and linearity. Therefore, it is crucial to study the sensing characteristics when these two optimization methods are combined.

In this work, we propose a dual-core D-shaped SPR-based PCF coated with a grating for refractive index sensing. Through a comparison between the original D-shaped PCF and the proposed structure, it has been demonstrated that the use of a dual-core enhances the excitation ratio, while the introduction of a grating improves the sensitivity. The working range can be optimized in the visible light wavelength region by optimizing structural parameters. A two-feature (2F) interrogation method was used to improve the sensing resolution. By taking advantage of the SPR effect occurring on the dual-core and grating, a reasonable sensor was used for refractive index detection of 1.33–1.37, with good linearity and resolution. The proposed performance has great potential for bio-sensing applications.

2. Design and Theoretical Method

The proposed structure consists of silica and a circular air hole with an external coating of gold grating and an analyte layer. By utilizing the stack-and-draw fabrication technique to fabricate the PCF, followed by side polishing, the PCF can be further processed using the electrochemical deposition method to construct the grating. As shown in Figure 1a, silica was used as the background material for the proposed PCF. The arrangement of the

air holes was formed by three rings of air holes, with two air holes removed in the second row. There were two types of air holes (large and small). The large holes help confine the light within the fiber core, while the small holes enable the light wave to penetrate and reach the metal-analyte interface, which excites more free electrons. An evanescent field can be easily produced due to the dual-core structure. Gold and silver films are the most suitable plasmonic materials for exciting SPR. While silver films may be more cost-effective to fabricate, gold films are typically preferred due to their chemical stability, as silver films are more susceptible to oxidation. Therefore, a gold film was coated on the flat surface of the proposed dual-core PCF. A gold grating was fabricated using photolithography, and the analyte was placed on the flat outer surface of the grating. The cross-section of the proposed D-shaped PCF is shown in Figure 1b. The polishing depth is $ds = 2.5 \mu\text{m}$, the pitch (distance between large holes) is $P = 1.9 \mu\text{m}$, the diameter of large holes is $d_1 = 0.95 \mu\text{m}$, the diameter of small holes is $d_2 = 0.475 \mu\text{m}$, the grating height is $h_g = 0.05 \mu\text{m}$, the grating period is $\Lambda = 1 \mu\text{m}$, and the duty ratio is $\eta = a/\Lambda = 0.5$ (a denotes the grating width). The analyte refractive index ranged from 1.33 to 1.37. The wavelength-dependent refractive index of the silica background is defined as [27].

$$n^2(\lambda) = 1 + \frac{A_1\lambda^2}{\lambda^2 - B_1^2} + \frac{A_2\lambda^2}{\lambda^2 - B_2^2} + \frac{A_3\lambda^2}{\lambda^2 - B_3^2} \tag{1}$$

where $A_1 = 0.6961663$, $A_2 = 0.4079426$, $A_3 = 0.8974794$, $B_1 = 0.0684043$, $B_2 = 0.1162424$, and $B_3 = 0.8974794$ are Sellmeier coefficients. The permittivity of gold can be obtained by Drude–Lorentz model and is defined as [28]:

$$\epsilon_m = \epsilon_\infty - \frac{\omega_D^2}{\omega(\omega + i\gamma_D)} - \frac{\Delta\epsilon \cdot \Omega_L^2}{(\omega^2 - \Omega_L^2) + i\Gamma_L\omega} \tag{2}$$

where ϵ_∞ is the metal permittivity, and $\epsilon_\infty = 5.9673$ for gold material. $\Delta\epsilon = 1.09$ is the weighting factor, $\omega_D/2\pi = 2113.6 \text{ THz}$ and $\gamma_D/2\pi = 15.92 \text{ THz}$ are the plasma frequency and damping frequency, respectively. $\Gamma_L/2\pi = 104.86 \text{ THz}$ and $\Omega_L/2\pi = 650.07 \text{ THz}$ are the spectral width and spectral frequency of the Lorentz oscillator, respectively. The loss can be defined as [29]:

$$\alpha = 8.686 \times \frac{2\pi}{\lambda} \text{Im}(n_{eff}) \times 10^4 \text{ dB/cm} \tag{3}$$

where λ is the light wavelength and $\text{Im}(n_{eff})$ is the imaginary part of the effective refractive index, and both L and λ are measured in the unit of dB/cm. The diffraction at a metallic diffraction grating provides excess in-plane momentum to compensate the wave vector mismatch between the incident wave and surface plasmon wave (SPW). The match condition of wave vector is expressed as [30]:

$$\pm k_0 \sqrt{\frac{\epsilon_m n_a^2}{\epsilon_m + n_a^2}} = k_0 n_a \sin \theta_{res} + m \frac{2\pi}{\Lambda} \tag{4}$$

where θ_{res} is the resonant angle of incidence, n_a is the refractive index of the analyte, which is in contact with the surface of the grating, m is an integer represent the diffraction order.

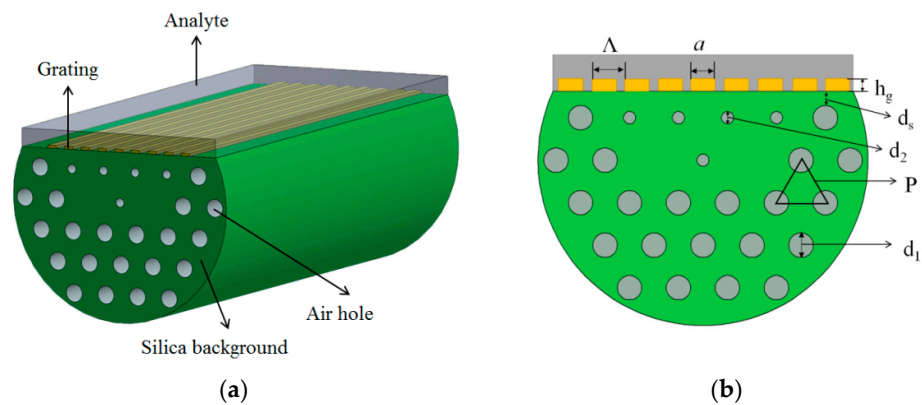


Figure 1. (a) The 3D view and (b) cross section of the proposed D-shaped PCF.

3. Results and Discussions

When the incident light is transmitted through the fiber core and a phase-matching condition is met, Spp is excited on the metal surface. The electric field of the core and Spp of the D-shaped PCF were simulated using FEM-based COMSOL Multiphysics software [31]. Figure 2 shows the simulation mesh division; a mesh composed of 15,306 domain elements and 985 boundary domain elements was constructed. Figure 3 depicts the relationship between the effective refractive index and the loss of the fundamental fiber core mode and Spp mode when the analyte has a refractive index of $n_e = 1.33$. When light propagates, if the direction of the electric field vibration does not change, the projection of the electric field in the xy plane will form a straight line, called linearly polarized light. If light enters the xz plane, it can be decomposed into two components. The polarized light generated on the x -axis is the TM wave, which is the p-polarized light; the polarized light generated on the y -axis is the TE wave, which is the s-polarized light. It can be seen that only the y-polarized mode is considered because the loss of the y-polarized mode is larger than the loss of the x-polarized mode. The effective refractive index curves of the Spp mode (black dotted line) and fundamental fiber core mode (black solid line) coincide at a wavelength of 708 nm. A sharp loss peak can be observed in the loss spectra of the core mode (red solid line) at the resonant wavelength, indicating that the maximum energy is transferred from the core mode to the Spp mode.

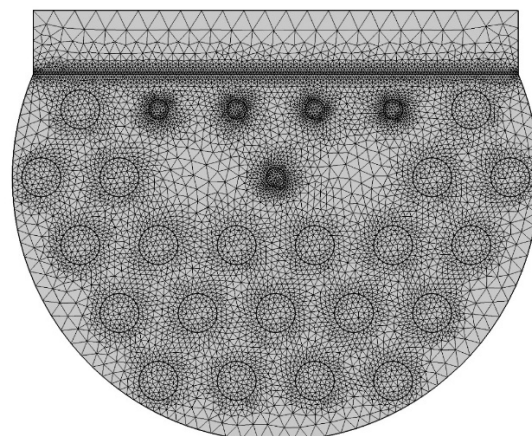


Figure 2. The mesh division of the proposed D-shaped PCF.

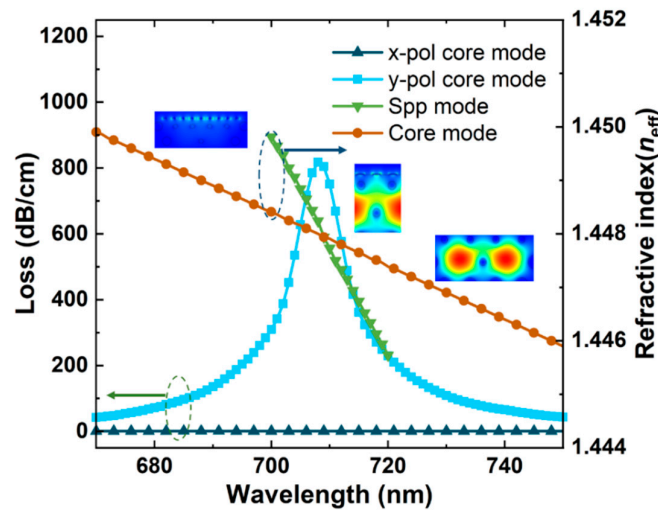


Figure 3. Dispersion relations of the fundamental fiber core mode and Spp mode at analyte $n_e = 1.33$.

3.1. Sensitivity

The effects of grating and dual-core structures on wavelength sensitivity and amplitude sensitivity were investigated, and the performance of the grating-assisted sensor was analyzed. The transmission spectra of the structures with and without gratings are shown in Figure 4a. The differences in the sensitivity between the two structures were compared. The wavelength sensitivity is denoted as [32–34]:

$$S_\lambda (\text{nm/RIU}) = \frac{\Delta\lambda_{\text{peak}}}{\Delta n_a} \tag{5}$$

where $\Delta\lambda_{\text{peak}}$ is the difference between the two resonant wavelengths and Δn_a is the change in the analyte refractive index. When the refractive index increases from 1.33 to 1.35, the resonant wavelength of the conventional structure is red-shifted from 606 nm to 612 nm for the gold film with a thickness of 50 nm. A sensitivity of 6 nm/0.02 RIU = 300 nm/RIU was achieved. Meanwhile, when the gold grating is coated on the flat surface of the dual-core D-shaped PCF, the resonant wavelength is red-shifted from 694 nm to 706 nm. In other words, a sensitivity of 600 nm/RIU can be obtained, which is two times that of a conventional structure. The response of the loss amplitude to the refractive index is also an important performance indicator. For the conventional structure, the loss changed from 42.247 dB/cm to 74.532 dB/cm when the refractive index increased from 1.33 to 1.35. The proposed structure exhibited a change in loss from 502.07 dB/cm to 993.25 dB/cm with the same refractive index variation (1.33 to 1.35). The amplitude sensitivity is denoted as [35]:

$$S_A (\text{RIU}^{-1}) = -\frac{1}{\alpha(\lambda, n_a)} \frac{\partial \alpha(\lambda, n_a)}{\partial n_a} \tag{6}$$

where $\alpha(\lambda, n_a)$ is the loss when the analyte refractive index is n_a and $\partial \alpha(\lambda, n_a)$ is the loss difference of two loss spectra due to adjacent analyte refractive indexes. The amplitude sensitivities of the conventional and proposed structures were computed using Equation (6). The resonance loss values at wavelengths $\lambda_1 = 606$ nm and $\lambda_2 = 694$ nm were used to compute the amplitude sensitivity. Theoretical calculation results in amplitude sensitivities of -28.82 RIU^{-1} and $-60.2869 \text{ RIU}^{-1}$ for the conventional and proposed structures, respectively. The results show that the wavelength and amplitude sensitivities can be enhanced by introducing a gold grating.

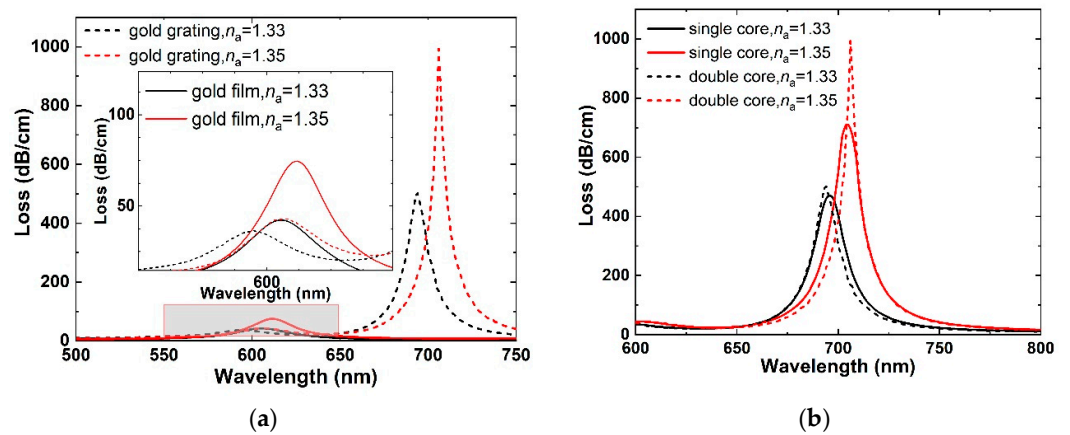


Figure 4. (a) Wavelength-dependent loss spectra of gold grating and gold film with refractive index from 1.33 to 1.35, and (b) Wavelength-dependent loss spectra of single-core and dual-core with refractive index from 1.33 to 1.35.

Using the same method, the role of the dual-core assisted sensor was analyzed. Figure 4b shows the variation in the transmission spectra of the single- and dual-core structures. For the single-core structure, the resonant wavelength difference was 8 nm, as the resonance wavelength was red-shifted from 696 nm to 704 nm, for the dual-core structure, a wavelength variation of 12 nm was observed, indicating that the wavelength sensitivities were 400 nm/RIU and 600 nm/RIU, respectively. Moreover, the amplitude sensitivities were 25.4776 RIU⁻¹ and 48.9044 RIU⁻¹. The results show that the dual-core can enhance the sensor performance, because of the changes of the refractive index can upon the energy between the two cores of the fiber directly [36].

From the above discussion, it is clear that gratings and dual-cores are two essential factors that promote sensor capability. Figure 5a shows the change in the loss peak as the analyte refractive index increases from 1.33 to 1.37. The resonance wavelength is red-shifted, the loss increases, and Table 1 shows the detailed changes, which are favorable for the detection of the analyte refractive. In addition, as the coupling efficiency between the core mode and Spp mode increases, more energy is transferred from the fiber core to the metal-dielectric interface, resulting in more peak loss. Figure 5b shows the amplitude (Amp.) sensitivity with the analyte refractive index variation from 1.33 to 1.37, and the maximal sensitivities of $-(1/130.75) \times [(130.75 - 275.69)/0.01] = 98.818$ RIU⁻¹, 126.493 RIU⁻¹, 156.065 RIU⁻¹, and 181.049 RIU⁻¹ are obtained by using Equation (6).

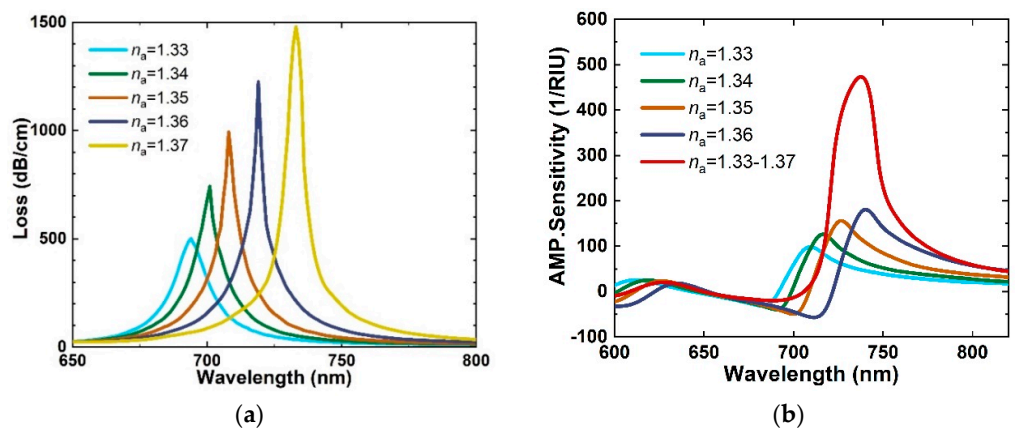


Figure 5. (a) Response curve of confinement loss as a function of wavelength for refractive index from 1.33 to 1.37, and (b) Amplitude sensitivity with varied refractive index.

Table 1. Changes of loss peak with different refractive indexes of the analyte.

RI of Analyte (RIU)	1.33	1.34	1.35	1.36	1.37
Wavelength (nm)	694.11	701.47	708.26	719.35	733.89
Loss (dB/cm)	502.07	743.33	993.25	1225.22	1480.66

3.2. Two-Feature (2F) Resolution

Two-feature (2F) sensitivity can be computed using Ref. [37], and is given by Equation (7).

$$S_{2F} = \frac{\sqrt{\Delta x^2 + \Delta y^2}}{\Delta n_a} \tag{7}$$

where $\Delta n_a = 0.02$ (1.33~1.35), $\Delta x = 14.15$ nm, and $\Delta y = 491.18$ dB/cm. The 2F sensitivity is higher than the single wavelength sensitivity and Amp. Sensitivity; however, the units of Δx and Δy are different. Therefore, the 2F resolution R_{2F} is used to describe the sensing performance, and it can be denoted as [37]:

$$R_{2F} = \frac{\Delta n_a}{\sqrt{\Delta I_x^2 + \Delta I_y^2}} \tag{8}$$

It is assumed that the minimum resolutions of the spectrometer are 0.02 nm and 0.05 dB (the sensing length of 1 cm). Approximately $\Delta I_x = \Delta x / 0.02$ nm = 707 change intervals in the wavelength and $\Delta I_y = \Delta y / 0.05$ dB = 9823 change intervals in the peak loss were obtained. The results show that $R_{2F} = 2.03 \times 10^{-6}$ RIU can be obtained, which is better than the 5.98×10^{-6} RIU (wavelength resolution) and 6.53×10^{-5} RIU (amplitude resolution).

Further, a comparison of the proposed work with the previous reports is made. Table 2 shows the sensing type, detection range, linearity, resolution, and related references.

Table 2. A comparison with previous reports.

Sensing Type	Detection Range	Linearity	Resolution (RIU)	Ref
All-glass endless single-mode PCF	1.33–1.37	0.9544	6.53×10^{-5}	[37]
D-shaped PCF with two micro-openings	1.33–1.37	0.9712	8.51×10^{-6}	[38]
Single-mode eccentric-core D-shaped PCF	1.33–1.37	0.9308	4.72×10^{-6}	[39]
D-shaped PCF with a gold layer covered by a TiO ₂ layer	1.36–1.41	0.9355	3.33×10^{-6}	[40]
Gold grating assisted D-shaped fiber	1.34–1.38	0.9890	1.31×10^{-5}	[41]
D-shaped PCF with graphene-gold deposited platform	1.33–1.39	0.9574	2.28×10^{-5}	[42]
Dual-core D-shaped PCF coated with gold grating	1.33–1.34	0.9742	2.075×10^{-6}	Present work
	1.34–1.35		1.998×10^{-6}	
	1.34–1.36		2.157×10^{-6}	
	1.36–1.37		1.956×10^{-6}	

The high sensitivity of the proposed structure is realized because of the common role of the dual-core structure, small air-holes, and grating. First, the design of the dual-core increases the effective interaction length of the core mode and Spp mode, and it reduces the average distance between the top edge of the core mode field and the interface of the gold metal, enhancing the coupling efficiency of the core mode and Spp mode. Second, when the small air-holes located above the top of the dual-core are kept fewer than the other holes, the mode field penetration gaps of the sensing channel become larger, which facilitates greater energy transfer to the cladding region. Third, evanescent waves can be enhanced by introducing a gold grating, which increases the sensitivity of the structure.

3.3. Investigation of the Proposed Sensor

The influence of the parameters of the proposed sensor on sensing performance was analyzed. In this section, two perspectives are discussed: the PCF structural parameters and gold grating structural parameters.

3.3.1. Effects of PCF Structural Parameters

It is necessary to ensure that the PCF structural parameters are based on practical PCF fabrication. Figure 6a shows the change in confinement loss with different polishing depths and that the loss peak of the fiber core mode is inextricably linked to the polishing depth. When the polishing depth increases from 2.1 μm to 2.9 μm , the resonance wavelength is blue-shifted, the loss peak of the fiber core first increases slightly from 967.31 dB/cm to 993.25 dB/cm, and then the loss peak decreases to 576.14 dB/cm because of the weak coupling between the fiber core mode and the Spp mode. The reason for the slightly increased loss at $d_s = 2.5 \mu\text{m}$ may be the improper mode guidance at the polishing depth. Therefore, considering that the fiber core can easily break at a smaller polishing depth, $d_s = 2.5 \mu\text{m}$ was used for further analysis. Figure 6b shows the change in confinement loss with different large hole diameters, d_1 , ranging from 0.6 μm to 1.4 μm . It can be observed that the diameter of the large holes has a slight influence on the confinement loss spectrum. The diameter $d_1 = 2.5 \mu\text{m}$ of the large holes is chosen because of the maximal loss. Figure 6c shows the change in the confinement loss with different small hole diameters, d_2 , ranging from 0.300 μm to 0.600 μm . The loss peak is red-shifted, and the phase-matching point moves towards the region of shorter wavelengths. The resonant wavelength $d_2 = 0.475 \mu\text{m}$ corresponds to the peak, which is because the ability to confine and store optical energy is weakened by the small holes.

3.3.2. Effects of Gold Grating Structural Parameters

The gold grating plays an important role in the improvement of sensing performance. Therefore, it is necessary to discuss the influence of the structural parameters of the grating on spectral changes. The variation of confinement loss with different grating heights is shown in Figure 7a. When the grating height increases from 0.03 μm to 0.07 μm , the resonance wavelength is blue-shifted from 749 nm to 681 nm, and the loss peak diminishes gradually from 1080.32 dB/cm to 881.41 dB/cm due to the higher damping loss. Around $h_g = 0.05 \mu\text{m}$, the variation of peak loss is found to be minimum, therefore, $h_g = 0.05 \mu\text{m}$ is taken for further analysis. This phenomenon occurs because as the grating height increases, more light energy from the fiber core is used to overcome the damping loss, resulting in a shift of the resonance wavelength towards a shorter wavelength. Figure 7b shows the change in confinement loss with different grating periods. With the increase in grating period from 0.6 μm to 1.4 μm , the resonance wavelength is red-shifted and accompanied by a variation in modal loss. The peak loss first increases up to $\Lambda = 1.0 \mu\text{m}$ and then decreases. A slight variation of peak loss is observed between $\Lambda = 0.8 \mu\text{m}$ and $\Lambda = 1.4 \mu\text{m}$. As the maximum loss was observed, $\Lambda = 1.0 \mu\text{m}$ was used for the following analysis. This phenomenon occurs because the grating period can modulate the resonance wavelength. Using the characteristic, D-shaped PCF sensors coated with gratings can operate at the expected wavelengths. Figure 7c shows the effect of the grating duty on the loss spectrum of the sensor. When the grating duty increases from 0.3 to 0.7, the resonance wavelength is red-shifted, and a sufficient increase in peak loss can be observed at $\eta = 0.5$. Therefore, $\eta = 0.5$ was taken to analyze the performance of the sensor. This phenomenon occurs because the resonance wavelength width and amplitude height are related to the fill factor of the grating. For example, in the fabrication of photoelectric devices, the ideal spectral curve can be obtained by tuning the grating duty.

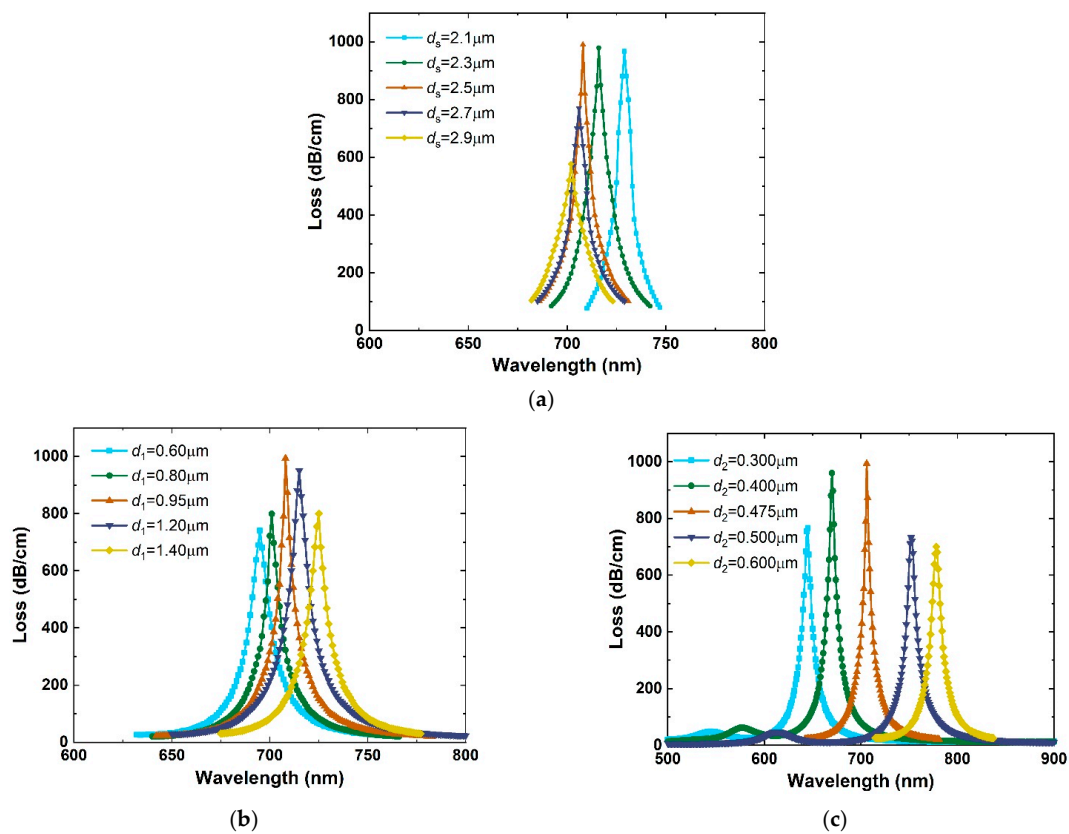


Figure 6. Response curve of confinement loss with (a) different polishing depths d_s , (b) the diameter of large hole d_1 , and (c) the diameter of small hole d_2 , for $n_a = 1.33$.

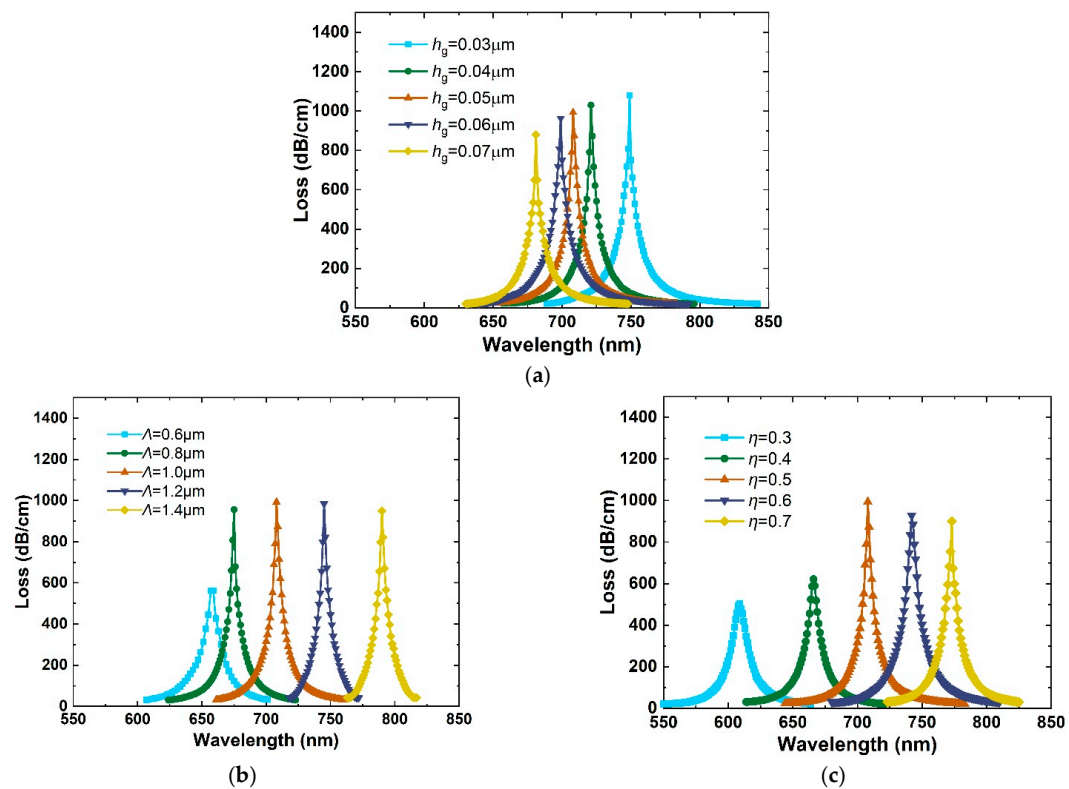


Figure 7. Response curve of confinement loss with different (a) grating heights h_g , (b) grating periods Λ , and (c) the grating duty η .

The structure of the proposed dual-core D-shaped PCF exhibited a better sensing performance than the original PCF, making it an ideal candidate for sensing external environment or biosensing application. The optical spectrum or sensitivity can be modified by changing the appropriate parameters.

In the current stage of the work, the performance parameters have already reached satisfactory levels, and further optimization of sensor parameters will be carried out in subsequent work.

4. Conclusions

A dual-core D-shaped photonic crystal fiber (PCF) surface plasmon resonance sensor coated with gold grating was proposed for refractive index measurements. Using the FEM, the optical sensing properties were analyzed in terms of wavelength and amplitude sensitivity. The effects of the proposed PCF structural parameters (polishing depth, diameter of the large holes, and diameter of the small holes) and the gold grating structural parameters (grating height, grating period, and grating duty) on the sensing performance were discussed. A refractive index sensing range of 1.33–1.37 was achieved in the visible region, and an average wavelength sensitivity of 994.5 nm/RIU. The amplitude sensitivity attained the highest value of 181.049 RIU⁻¹ with an analyte refractive index of 1.37. Further, a 2F interrogation method was used to improve the performance. Compared with the original PCF, the optical sensing response indicates that the proposed PCF sensor is a potential candidate for application in water quality testing, biochemical sensing, and external environmental monitoring. Similarly, there were benefits to the appropriate operating wavelength and sensitivity. This work is a promising candidate in the field of laser, sensor, and optical communication systems.

Author Contributions: Writing—original draft, Y.Y.; resources, Y.X.; software, S.C. and D.S.; supervision, Z.G.; writing—review & editing, G.S.; data curation, X.T. All authors have read and agreed to the published version of the manuscript.

Funding: This work was supported by the National Natural Science Foundation of China (Grant No. 62273243 and 62003225) and the Applied Basic Research Programs of Liao Ning (Grant No. 2022020341-JH2/1013).

Institutional Review Board Statement: Not applicable.

Informed Consent Statement: Not applicable.

Data Availability Statement: Not applicable.

Conflicts of Interest: The authors declare no conflict of interest.

References

1. Islam, M.R.; Khan, M.M.I.; Siraz, S.; Mehjabin, F.; Rahman, M.; Islam, M.; Anzum, M.S.; Chowdhury, J.A.; Noor, F. Design and analysis of a QC-SPR-PCF sensor for multipurpose sensing with supremely high FOM. *Appl. Nanosci.* **2022**, *12*, 29–45. [[CrossRef](#)]
2. El-Saeed, A.H.; Khalil, A.E.; Hameed, M.F.O.; Azab, M.Y.; Obayya, S.S.A. Highly sensitive SPR PCF biosensors based on Ag/TiN and Ag/ZrN configurations. *Opt. Quantum Electron.* **2019**, *51*, 56. [[CrossRef](#)]
3. Kaur, V.; Singh, S. Design of titanium nitride coated PCF-SPR sensor for liquid sensing applications. *Opt. Fiber Technol.* **2019**, *48*, 159–164. [[CrossRef](#)]
4. Mittal, S.; Sharma, T.; Tiwari, M. Surface plasmon resonance based photonic crystal fiber biosensors: A review. *Mater. Today Proc.* **2021**, *43*, 3071–3074. [[CrossRef](#)]
5. Paul, A.K.; Sarkar, A.K.; Khaleque, A. Dual-core photonic crystal fiber plasmonic refractive index sensor: A numerical analysis. *Photonic Sens.* **2019**, *9*, 151–161. [[CrossRef](#)]
6. Li, J.; Chen, G.; Meng, F. A fiber-optic formic acid gas sensor based on molybdenum disulfide nanosheets and chitosan works at room temperature. *Opt. Laser Technol.* **2022**, *150*, 107975. [[CrossRef](#)]
7. Wang, D.; Yi, Z.; Ma, G.; Dai, B.; Yang, J.; Zhang, J.; Yu, Y.; Liu, C.; Wu, X.; Bian, Q. Two-channel photonic crystal fiber based on surface plasmon resonance for magnetic field and temperature dual-parameter sensing. *Phys. Chem. Chem. Phys.* **2022**, *24*, 21233–21241. [[CrossRef](#)]
8. Zhu, W.; Yi, Y.; Yi, Z.; Bian, L.; Yang, H.; Zhang, J.; Yu, Y.; Liu, C.; Li, G.; Wu, X. High confidence plasmonic sensor based on photonic crystal fibers with a U-shaped detection channel. *Phys. Chem. Chem. Phys.* **2023**, *25*, 8583–8591. [[CrossRef](#)]

9. Nielsen, M.D.; Mortensen, N.A. Photonic crystal fiber design based on the V-parameter. *Opt. Express* **2003**, *11*, 2762–2768. [[CrossRef](#)]
10. Uniyal, A.; Srivastava, G.; Pal, A.; Taya, S.; Muduli, A. Recent Advances in Optical Biosensors for Sensing Applications: A Review. *Plasmonics* **2023**, *18*, 735–750. [[CrossRef](#)]
11. Karki, B.; Jha, A.; Pal, A.; Srivastava, V. Sensitivity enhancement of refractive index-based surface plasmon resonance sensor for glucose detection. *Opt. Quantum Electron.* **2022**, *54*, 595. [[CrossRef](#)]
12. Rifat, A.A.; Ahmed, R.; Yetisen, A.K.; Butt, H.; Sabouri, A.; Mahdiraji, G.A.; Yun, S.H.; Adikan, F.M. Photonic crystal fiber based plasmonic sensors. *Sens. Actuators B Chem.* **2017**, *243*, 311–325. [[CrossRef](#)]
13. Zhao, Y.; Tong, R.-J.; Xia, F.; Peng, Y. Current status of optical fiber biosensor based on surface plasmon resonance. *Biosens. Bioelectron.* **2019**, *142*, 111505. [[CrossRef](#)] [[PubMed](#)]
14. Yesudasu, V.; Pradhan, H.S.; Pandya, R.J. Recent progress in surface plasmon resonance based sensors: A comprehensive review. *Heliyon* **2021**, *7*, e06321. [[CrossRef](#)] [[PubMed](#)]
15. Popescu, V.; Sharma, A.K.; Marques, C. Resonant interaction between a core mode and two complementary supermodes in a honeycomb PCF reflector-based SPR sensor. *Optik* **2021**, *227*, 166121. [[CrossRef](#)]
16. Chaudhary, V.S.; Kumar, D.; Kumar, S. Gold-immobilized photonic crystal fiber-based SPR biosensor for detection of malaria disease in human body. *IEEE Sens. J.* **2021**, *21*, 17800–17807. [[CrossRef](#)]
17. Wang, J.; Pei, L.; Wu, L.; Wang, J.; Ruan, Z.; Zheng, J. A polarization-independent SPR sensor based on photonic crystal fiber for low RI detection. *Plasmonics* **2020**, *15*, 327–333. [[CrossRef](#)]
18. Chaudhary, V.S.; Kumar, D.; Kumar, S. SPR-assisted photonic crystal fiber-based dual-wavelength single polarizing filter with improved performance. *IEEE Trans. Plasma Sci.* **2021**, *49*, 3803–3810. [[CrossRef](#)]
19. Guo, Z.; Fan, Z.; Kong, X.; Meng, Z. Photonic crystal fiber based wide-range of refractive index sensor with phase matching between core mode and metal defect mode. *Opt. Commun.* **2020**, *461*, 125233. [[CrossRef](#)]
20. Yang, H.; Wang, G.; Lu, Y.; Yao, J. Highly sensitive refractive index sensor based on SPR with silver and titanium dioxide coating. *Opt. Quantum Electron.* **2021**, *53*, 341. [[CrossRef](#)]
21. Ying, Y.; Si, G.-Y.; Luan, F.-J.; Xu, K.; Qi, Y.-W.; Li, H.-N. Recent research progress of optical fiber sensors based on D-shaped structure. *Opt. Laser Technol.* **2017**, *90*, 149–157. [[CrossRef](#)]
22. Sakib, M.N.; Hossain, M.B.; Al-tabatabaie, K.F.; Mehedi, I.M.; Hasan, M.T.; Hossain, M.A.; Amiri, I.S. High performance dual core D-shape PCF-SPR sensor modeling employing gold coat. *Results Phys.* **2019**, *15*, 102788. [[CrossRef](#)]
23. Jabin, M.A.; Ahmed, K.; Rana, M.J.; Paul, B.K.; Luo, Y.; Vigneswaran, D. Titanium-coated dual-core D-shaped SPR-based PCF for hemoglobin sensing. *Plasmonics* **2019**, *14*, 1601–1610. [[CrossRef](#)]
24. Singh, S.; Prajapati, Y.K. Highly sensitive dual-core symmetrical side-polished modified D-shaped SPR based PCF refractive index sensor with deeply etched micro openings. *Optik* **2021**, *235*, 166657. [[CrossRef](#)]
25. Lu, J.; Li, Y.; Han, Y.; Liu, Y.; Gao, J. D-shaped photonic crystal fiber plasmonic refractive index sensor based on gold grating. *Appl. Opt.* **2018**, *57*, 5268–5272. [[CrossRef](#)] [[PubMed](#)]
26. Fang, H.; Wei, C.; Yang, H.; Zhao, B.; Yuan, L.; Li, J. D-Shaped Photonic Crystal Fiber Plasmonic Sensor Based on Silver-Titanium Dioxide Composite Micro-grating. *Plasmonics* **2021**, *16*, 2049–2059. [[CrossRef](#)]
27. Wang, Q.; Jing, J.Y.; Wang, X.Z.; Niu, L.Y.; Zhao, W.M. A D-shaped fiber long-range surface plasmon resonance sensor with high Q-factor and temperature self-compensation. *IEEE Trans. Instrum. Meas.* **2019**, *69*, 2218–2224. [[CrossRef](#)]
28. Dong, Y.; Wu, B.; Wang, M.; Xiao, H.; Xiao, S.; Sun, C.; Li, H.; Jian, S. Magnetic field and temperature sensor based on D-shaped fiber modal interferometer and magnetic fluid. *Opt. Laser Technol.* **2018**, *107*, 169–173. [[CrossRef](#)]
29. Li, J.; Liu, B.; Liu, J.; Shi, J.-L.; He, X.-D.; Yuan, J.; Wu, Q. Low-cost wearable device based D-shaped single mode fiber curvature sensor for vital signs monitoring. *Sens. Actuators A Phys.* **2022**, *337*, 113429. [[CrossRef](#)]
30. Lin, K.; Lu, Y.; Chen, J.; Zheng, R.; Wang, P.; Ming, H. Surface plasmon resonance hydrogen sensor based on metallic grating with high sensitivity. *Opt. Express* **2008**, *16*, 18599–18604. [[CrossRef](#)]
31. Pathak, A.K.; Singh, V.K. SPR based optical fiber refractive index sensor using silver nanowire assisted CSMFC. *IEEE Photonics Technol. Lett.* **2020**, *32*, 465–468. [[CrossRef](#)]
32. Zhu, L.; Zhao, N.; Lin, Q.; Zhao, L.; Jiang, Z. Optical fiber SPR magnetic field sensor based on photonic crystal fiber with the magnetic fluid as cladding. *Meas. Sci. Technol.* **2021**, *32*, 075106. [[CrossRef](#)]
33. D’Amico, A.; Di Natale, C. A contribution on some basic definitions of sensors properties. *IEEE Sens. J.* **2001**, *1*, 183–190. [[CrossRef](#)]
34. Huang, Q.; Zeng, D.; Li, H.; Xie, C. Room temperature formaldehyde sensors with enhanced performance, fast response and recovery based on zinc oxide quantum dots/graphene nanocomposites. *Nanoscale* **2012**, *4*, 5651–5658. [[CrossRef](#)]
35. Divya, J.; Selvendran, S.; Raja, A.S.; Sivasubramanian, A. Graphene-Au-Coated Plasmonic Sensor Based on D-Shaped Bezier Polygonal Hollow Core Photonic Crystal Fiber. *Braz. J. Phys.* **2021**, *51*, 1314–1323. [[CrossRef](#)]
36. An, G.; Li, S.; Yan, X.; Zhang, X.; Yuan, Z.; Zhang, Y. High-sensitivity and tunable refractive index sensor based on dual-core photonic crystal fiber. *J. Opt. Soc. Am. B* **2016**, *33*, 1330–1334. [[CrossRef](#)]
37. Chen, Y.; Xie, Q.; Li, X.; Zhou, H.; Hong, X.; Geng, Y. Experimental realization of D-shaped photonic crystal fiber SPR sensor. *J. Phys. D Appl. Phys.* **2016**, *50*, 025101. [[CrossRef](#)]

38. Zhang, S.; Li, J.; Li, S.; Liu, Q.; Wu, J.; Guo, Y. Surface plasmon resonance sensor based on D-shaped photonic crystal fiber with two micro-openings. *J. Phys. D Appl. Phys.* **2018**, *51*, 305104. [[CrossRef](#)]
39. Falah, A.A.S.; Wong, W.R.; Adikan, F.R.M. Single-mode eccentric-core D-shaped photonic crystal fiber surface plasmon resonance sensor. *Opt. Laser Technol.* **2022**, *145*, 107474. [[CrossRef](#)]
40. Gangwar, R.K.; Amorim, V.A.; Marques, P.V.S. High performance titanium oxide coated D-shaped optical fiber plasmonic sensor. *IEEE Sens. J.* **2019**, *19*, 9244–9248. [[CrossRef](#)]
41. Khanikar, T.; Singh, V.K. Gold grating assisted SPR based D-shaped single mode fiber for detection of liquid refractive index. *Opt. Quantum Electron.* **2019**, *51*, 296. [[CrossRef](#)]
42. An, G.; Li, S.; Cheng, T.; Yan, X.; Zhang, X.; Zhou, X.; Yuan, Z. Ultra-stable D-shaped optical fiber refractive index sensor with graphene-gold deposited platform. *Plasmonics* **2019**, *14*, 155–163. [[CrossRef](#)]

Disclaimer/Publisher’s Note: The statements, opinions and data contained in all publications are solely those of the individual author(s) and contributor(s) and not of MDPI and/or the editor(s). MDPI and/or the editor(s) disclaim responsibility for any injury to people or property resulting from any ideas, methods, instructions or products referred to in the content.